Intracellular Precipitation of Pb by Shewanella putrefaciens CN32 during the Reductive Dissolution of Pb-Jarosite

ARTICLE *in* ENVIRONMENTAL SCIENCE AND TECHNOLOGY · NOVEMBER 2009

Impact Factor: 5.33 · DOI: 10.1021/es901629c · Source: PubMed

3 AUTHORS:

Christina M Smeaton
University of Waterloo
9 PUBLICATIONS **38** CITATIONS
SEE PROFILE

Brian J Fryer
University of Windsor
199 PUBLICATIONS **5,890** CITATIONS
SEE PROFILE

C. G. Weisener
University of Windsor
57 PUBLICATIONS **838** CITATIONS
SEE PROFILE

Environ. Sci. Technol. **2009,** *43,* 8086–8091

Intracellular Precipitation of Pb by *Shewanella putrefaciens* CN32 during the Reductive Dissolution of Pb-Jarosite

CHRISTINA M. SMEATON,*
BRIAN J. FRYER, AND
CHRISTOPHER G. WEISENER
Great Lakes Institute for Environmental Research, University of Windsor, Windsor, Ontario, Canada, N9B 3P4

Received June 3, 2009. Revised manuscript received August 24, 2009. Accepted September 9, 2009.

Jarosites ($MFe_3(SO_4)_2(OH)_6$) are precipitated in the Zn industry to remove impurities during the extraction process and contain metals such as Pb and Ag. Jarosite wastes are often confined to capped tailings ponds, thereby creating potential for anaerobic reductive dissolution by microbial populations. This study demonstrates the reductive dissolution of synthetic Pb-jarosite ($PbFe_6(SO_4)_4(OH)_{12}$) by a subsurface dissimilatory Fe reducing bacterium (*Shewanella putrefaciens* CN32) using batch experiments under anaerobic circumneutral conditions. Solution chemistry, pH, Eh, and cell viability were monitored over time and illustrated the reduction of released structural Fe(III) from the Pb-jarosite to Fe(II). Inoculated samples containing Pb-jarosite also demonstrated decreased cellular viability coinciding with increased Pb concentrations. SEM images showed progressive nucleation of electron dense nanoparticles on the surface of bacteria, identified by TEM/EDS as intracellular crystalline precipitates enriched in Pb and P. The intracellular precipitation of Pb by *S. putrefaciens* CN32 observed in this study provides potential new insight into the biogeochemical cycling of Pb in reducing environments.

Introduction

Plumbojarosite ($PbFe_6(SO_4)_4(OH)_{12}$) was first described in 1902 at Cook's Peak, New Mexico and often forms during the oxidation of sulfide deposits (*1, 2*). In these environments, Pb mobility is limited by the low solubility of anglesite ($PbSO_4$, $\log K_{sp} = -7.7$) and cerrusite ($PbCO_3$, $\log K_{sp} = -12.8$), consequently plumbojarosite ($\log K_{sp} = -16.8$) is often the last mineral to form (*1, 3*). Plumbojarosite is thermodynamically stable up to pH 5 under high Fe and sulfate concentrations typical of acid mine drainage (AMD) environments and is suggested to control aqueous Pb mobility at these sites (*2*−*4*). At pH values above 5.0, plumbojarosite is subject to dissolution/reprecipitation reactions and may form Fe oxides or hydroxides (*5*). Under these conditions, Fe hydroxides such as ferrihydrite become important scavengers of Pb.

Structurally, plumbojarosite or Pb-jarosite (i.e., synthetic analog) is a member of the alunite-jarosite mineral super group with the general formula $AB_3(TO_4)_2(OH)_6$. The A sites are occupied by monovalent (e.g., K and Na) and divalent cations (e.g., Ca(II), Pb(II), and Ag(II)). The B position corresponds to cation sites with octahedral (O) coordination, typically Al(III) or Fe(III), while the T position corresponds to tetrahedral (T) coordination (e.g., S(VI), As(V)) (*6*). Over the past 20 years, the Zn industry has capitalized on the stability of jarosite minerals and during the metal extraction process, synthetic jarosites are purposely precipitated to remove unwanted impurities such as Fe, sulfates, alkalis, and other heavy metals (e.g., Pb, Ag). Jarosite precipitation is advantageous because the precipitates are easily filtered and give low losses of Zn metal, therefore, this process accounts for 80% of all Zn extracted worldwide (8 Mt/yr) (*1*). The majority of the precipitates contain Na and K jarosite, however, Pb-jarosite will form during the acid pressure leaching of Pb-containing Zn concentrates (*1*). While the jarosite process is a highly efficient and economical method to optimize Zn recoveries, it also produces large volumes of wastes. For example, a plant annually producing 150 000 tonnes of metallic Zn will generate approximately 125 000 tonnes of jarosite (*1*). Jarositic wastes are not easily recyclable and may contain elevated concentrations of toxic heavy metals such as Pb, therefore the safe disposal of these wastes is of paramount concern.

One of the most widely used storage method is disposal in lined ponds under circumneutral conditions (*1*). However, despite the environmental relevance of jarosite minerals, few studies have evaluated the abiotic or biotic dissolution of jarosites under these storage conditions (*5, 7*−*10*). Therefore, the primary objective of this study was to assess the effects of a model metal reducing bacterium, *Shewanella putrefaciens* CN32, on the dissolution of synthetic Pb-jarosite under circumneutral anaerobic conditions. *S. putrefaciens* CN 32 was chosen because it is a well characterized subsurface chemoautotrophic anaerobe capable of using Fe(III) during dissimilatory iron reduction (*11*−*13*). A secondary objective of this study was to evaluate the fate and toxicological effects of the Pb released during the dissolution experiment on *S. putrefaciens* CN32. To the best of our knowledge, this is the first study to assess the fate of Pb during Pb-jarosite/microbe interactions.

Materials and Methods

Preparation of the Pb-Jarosite/Cell Suspensions and Sampling Procedures. Pb-jarosite was synthesized as per the method used by Dutrizac et al. (*14, 15*). (see Supporting Information (SI) Section 1 for more details). Pure cultures of *S. putrefaciens CN32* were grown, harvested, and inoculated into a modified M1 minimal media (SI Section S2). The inoculated minimal media was transferred to an anaerobic chamber (96% N_2/4% H_2) and 16 mL aliquots were added to 20 mL polypropylene test tubes containing 0.0500 ± 0.0013 g of Pb-jarosite (33 samples). Experimental controls contained 16 mL of sterile minimal media in 20 mL polypropylene tubes containing 0.0500 ± 0.0013 g of Pb-jarosite (33 samples). To monitor background elemental concentrations over time, an additional set of test tubes were prepared containing only the inoculated minimal media (10 samples) and sterile minimal media (10 samples). All samples were capped, sealed, and rotated end-over-end in the anaerobic chamber. Samples containing Pb-jarosite were removed in triplicate from the rotator at 0, 6, 16, 24, 38, 48, 72, 120, 192, 408, 768 h, whereas minimal media samples (i.e., in the absence of Pb-jarosite) were removed from the rotator in duplicate at 0, 48, 192, 408, 768 h. All samples were monitored for Eh and pH using semimicro electrodes, and aqueous concentrations of Pb, Fe, and S were determined using inductively coupled plasma optical emission spectroscopy (ICP-OES) (SI Section S3).

* Corresponding author phone: (519) 253-3000ext. 4246; fax: (519) 971-3616; e-mail: smeato3@uwindsor.ca.

10.1021/es901629c CCC: $40.75

Published on Web 09/24/2009

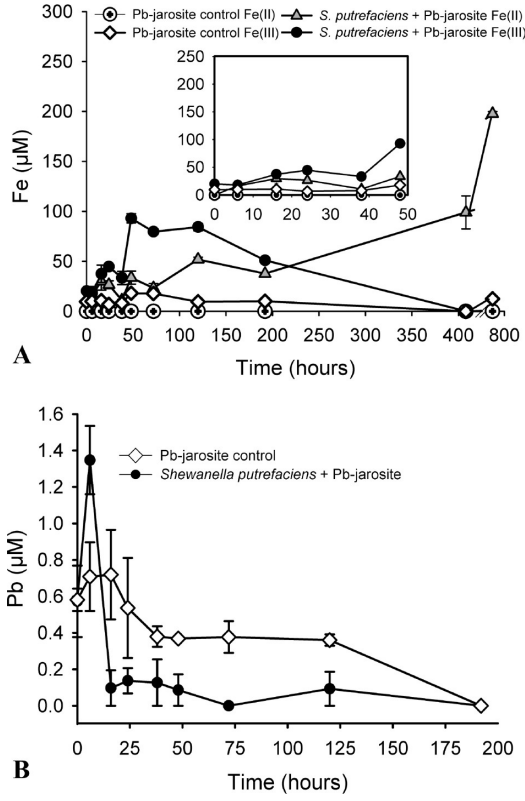

FIGURE 1. (A) Aqueous Fe(II) and Fe(III) release in the control and inoculated Pb-jarosite samples as a function of time; (B) Aqueous Pb release in the control and inoculated Pb-jarosite samples as a function of time. Error bars represent standard error ($n = 3$).

Duplicate volumes of the remaining filtrate (100 μL) were used to immediately determine Fe(II) and total Fe concentrations via the ferrozine method (*16, 17*). Fe(III) concentrations were determined by subtracting Fe(II) concentrations from total Fe concentrations. The pH, Eh, minimal media composition and measured aqueous concentrations of Fe(II), Fe(III), and Pb were used to calculate equilibrium aqueous activities and saturation indices for the both the control and inoculated dissolution experiments using the Geochemist's Workbench (GWB, version 7.01).

Slurries from each sample were collected at each sampling period and imaged immediately (i.e., usually within 2 h) using field emission-environmental scanning electron microscopy (FE-ESEM) (SI Section 4). An additional set of 1.0 mL slurries were collected for TEM preparation and analysis (SI Section S5).

Cell Viability. A 1.0 mL slurry from each sample (i.e., including controls) was collected and analyzed for cell viability using the Promega BacTiter-Glo microbial cell viability assay and reported as relative luciferase units (RLU) (SI Section S6).

Results and Discussion

Control Experiments. Aqueous Fe(II), Fe(III), and Pb concentrations were below detection limits in all sterile and inoculated samples (i.e., in the absence of Pb-jarosite). In the control samples containing Pb-jarosite, aqueous Fe(III) release was minimal and reached a maximum at 48 h of $18.01 \pm 0.80\,\mu$M at a release rate of $0.10 \pm 0.3.0\,\mu$M/h followed by a decrease in Fe(III) concentrations (Figure 1A). The concentration of S was 56.0 mM due to the PIPES buffer, and remained constant throughout the experiment in all samples and could not be used to evaluate Pb-jarosite dissolution. Aqueous Pb concentrations in the control samples reached a maximum at $0.70 \pm 0.41\,\mu$M at 6 h followed by a steady decrease at a rate of $1.3 \times 10^{-3} \pm 1.0 \times 10^{-3}\,\mu$M/h to 198 h (Figure 1B). Beyond 198 h, all samples were below the instrumental Pb detection limit (0.09 μM). Aqueous Fe and Pb concentrations reported by Smith et al. (*5*) for the abiotic dissolution of Pb-jarosite under comparable conditions were mass normalized and showed lower concentrations of Fe (3.90 μM) and slightly higher concentrations of Pb (3.3 μM) at 750 h. The minimal aqueous Fe released reported in this study and by Smith et al. (*5*) is likely due to the stability of the FeO_6 octahedra within the tetrahedral-octahedral-tetrahedral (T-O-T) jarosite structure.

The observed decrease in aqueous Fe and Pb concentrations in this study after 48 h likely resulted from the precipitation of a secondary mineral phase. Secondary electron SEM images of the Pb-jarosite control samples at 408 h (SI Figure S2A) showed spherical precipitates on the surface of the Pb-jarosite, similar in morphology to those previously observed and identified as $Fe(OH)_3$ during Pb-jarosite dissolution (*5*). Energy dispersive X-ray (EDX) spectra measured at 20 kV demonstrated the change in relative elemental concentrations from (Fe = 24.0 wt %, Pb = 13.8 wt %, S = 13.4 wt %, O = 48.7 wt %) on the surface of the Pb-jarosite to (Fe = 46.1 wt %, Pb = 28.2 wt %, S = 11.7 wt %, O = 14.1 wt %) on the thickest part of the precipitate thereby suggesting possible Fe and Pb remineralization (SI Figure S3). React (GWB 7.01) calculated saturation indices (log Q/K) at 0 and 48 h based on experimental data (SI Table S1) and predicted the precipitation of hematite, goethite and $Fe(OH)_3$ (SI Table S2). Hematite was discounted as a potential precipitate because it is a highly crystalline phase, typically formed over longer durations (*18*). The predicted formation of goethite or $Fe(OH)_3$ is significant because these phases represent important sinks for Pb sorption in the environment and may account for the enrichment of Pb observed in the EDX measurements.

Microbial Reduction of Pb-Jarosite. Aqueous Fe(II) and Fe(III) concentrations were monitored over time to evaluate the susceptibility of Pb-jarosite to microbial Fe reduction. The release of Fe(III) was higher in the inoculated Pb-jarosite samples as compared to the control samples (Figure 1A). A maximum Fe(III) concentration of $93.0 \pm 7.94\,\mu$M at a rate of $12.1 \pm 1.28\,\mu$M/h was reached at 48 h followed by a gradual decrease to $12.4 \pm 1.89\,\mu$M at 776 h (Figure 1A). The reduction of Fe(III) within these samples was first observed during the second sampling interval (6 h) with a release of 16.4 μM Fe(II) which continued to increase to $197.1 \pm 2.92\,\mu$M at a rate of $3.9 \times 10^{-1}\,\mu$M/h until the termination of the experiment (768 h) (Figure 1A). The first observation of Fe(III) reduction also corresponded to a maximum increase of aqueous Pb concentrations from $0.57 \pm 0.34\,\mu$M at time 0 to 1.35 ± 0.26 μM at 6 h, likely due to structural Pb release from the Pb-jarosite during dissimilatory Fe reduction (Figure 1B). The increase in Pb concentrations was followed by a sharp decrease to 0.097 μM at a slow release rate of $6.0 \times 10^{-4} \pm 7.0 \times 10^{-4}\,\mu$M/h to198 h at which point aqueous Pb concentrations were below detection limits (Figure 1B). The rate of Fe reduction increased substantially between 192 and 400 h when aqueous Fe(II) concentrations increased from $37.5 \pm 2.35\,\mu$M at 198 h to $98.9 \pm 23.4\,\mu$M at 400 h (Figure 1A). The observed shift to Fe reduction in the inoculated Pb-jarosite samples also coincided with a decrease in redox potential from +84.46 mV at 192 h to −84.26 mV at 408 h, not observed in the inoculated minimal media control samples in the absence of Pb-jarosite (SI Figure S4).

Secondary electron images of secondary precipitates observed on the surface of the Pb-jarosite at 408 h showed spherical precipitates similar to those seen in the control samples (SI Figure S2B). Geochemical modeling was divided into two parts (i.e., 0−48 h and 48−768 h) to reflect the

changes in Fe(II) and Fe(III) concentrations over time. Based on reaction path modeling, React (GWB 7.01) calculated saturation indices (log Q/K) over time using the minimal media composition and experimental data collected at 0, 48, and 768 h (SI Table S3) and predicted the initial precipitation of hematite > goethite > magnetite> carbonate green rust (SI Table S4). However, as the reaction progressed and Fe(III) decreased and Fe(II) increased, React predicted the precipitation of carbonate green rust > sulfate green rust> chloride green rust > hematite > magnetite (SI Table S4). Green rusts are mixed Fe(II)/Fe(III) hydroxides that typically form under weakly acidic and alkaline suboxic environments and were formed in previous studies by *S. putrefaciens* CN32 during the dissimilatory Fe reduction of ferrihydrite and lepidocrocite (*13, 19*). However, the secondary precipitates formed in this study do not exhibit the characteristic hexagonal platelet morphology typical of green rusts. Moreover, Fredrickson et al. (*13*) demonstrated magnetite formation over the formation of green rusts in the absence of P by *S. putrefaciens* CN32 during dissimilatory Fe reduction. Therefore, it is unlikely that carbonate green rust formed during these experiments and it is more likely that magnetite or an Fe hydroxide such as goethite was formed.

The absence of P in the minimal media and the presence of aqueous Pb may have played an important role in the low concentrations of aqueous Fe(II) observed throughout the experiment as both have previously demonstrated inhibitory effects on Fe reduction in Fe(hydr)oxides by *S. putrefaciens* (*20, 21*). While dissimilatory iron reduction of various synthetic Fe (hydr)oxides has been studied extensively, few studies have examined the dissimilatory Fe reduction of jarosite minerals. Recently, Weisener et al. (*10*) demonstrated Fe reduction during silver jarosite, $AgFe_3(SO_4)_2(OH)_6$ dissolution in the presence of *S. putrefaciens* CN32 under comparable conditions and showed a maximum aqueous Fe(II) concentration of 167.0 μM at 168 h. Similarly, Jones et al. (*22*) also demonstrated Fe reduction from jarosite, $KFe_3(SO_4)_2(OH)_6$, using *Geobacter metallireducens* GS-15 and *Geobacter sp.* ENN 1.

To evaluate the potential effects of the Pb released during Pb-jarosite dissolution on *S. putrefaciens*, cell viability was monitored in inoculated samples in both the presence and absence of Pb-jarosite and reported as luminescence (RLU). Initially, luminosity was higher in the inoculated Pb-jarosite samples ($1.49 \times 10^6 \pm 7.81 \times 10^4$ RLU) compared to the inoculated minimal media samples ($8.81 \times 10^5 \pm 1.62 \times 10^4$ RLU) after 48 h thus suggesting greater cell viability at the beginning of the experiment in samples containing Pb-jarosite (SI Figure S5). The greater cell viability initially observed in the inoculated samples containing Pb-jarosite corresponded with increased Fe(III) release and subsequent Fe(II) production and was likely due to increased metabolic activity due to dissimilatory Fe reduction (Figure 1A). However at 72 h, cell viability in the inoculated samples containing Pb-jarosite ($7.91 \times 10^6 \pm 2.23 \times 10^5$ RLU) decreased while cell viability in the inoculated samples without Pb-jarosite ($6.92 \times 10^6 \pm 2.63 \times 10^4$ RLU) demonstrated larger luminescence (i.e., cell viability) and continued to increase until 198 h (SI Figure S5). The decrease in cell viability observed earlier in the inoculated samples containing Pb-jarosite was likely due to the presence of aqueous Pb released during Pb-jarosite dissolution (Figure 1) (*20, 21*).

Fate of Pb. Back scattered electron (BSE)-SEM images taken within 2 h of sampling demonstrated progressive nanoparticle formation over time indicated by high contrast spots associated with the cell surface (Figure 2B, D, F) not observed in the control experiments (Figure 2A, C, E). The diameter of the electron dense particles associated with the cell surface were measured using the Scandium SEM image platform, and the mean diameter of the each particle was 113.20 nm ($n = 13$, SD = 29.59 nm).While BSE-SEM images suggest extracellular precipitation, TEM images collected on a cross section of an individual cell at 406 h (Figure 3A) demonstrated intracellular accumulation of electron dense granules within the cytoplasm and were observed in the many of the cells imaged (SI Figure S6A). The appearance of extracellular precipitation of the electron dense nanoparticles during BSE-SEM not seen in the TEM images is likely the result of cellular dehydration under low vacuum (80 Pa). The progressive increase in electron dense nanoparticles over time associated with the cells (Figure 2A, C, E) coincided with decreased aqueous Pb concentrations thus suggesting the precipitation of an enriched Pb phase (Figure 1B). In addition to typical cellular components such as C and S, TEM-EDS analyses of the electron dense granules (i.e., spots 1−3) showed enrichment of Pb (90.38−92.74 wt %) and P (1.76−2.26 wt %) (SI Table S5). EDS analyses also showed residual Ca (0.46−0.56 wt %) not seen in any other cellular components. The cytoplasm (i.e., spot 4) in the absence of electron dense particles was primarily composed of C (95.58 wt %) and showed residual Pb (0.98 wt %) thus demonstrating transport of Pb into the cytoplasm likely followed by precipitation of the electron dense Pb rich granules. EDS analysis of the cell wall (i.e., spot 5) showed Pb enrichment (5.71 wt %) and is likely due to the formation of adsorption complexes with carboxyl and phosphoryl functional groups commonly reported at neutral pH values (*23, 24*). In addition to Pb, the cell wall (i.e., spot 5) was also enriched in C (89.38 wt %) and Fe (11.67 wt %) with lower concentrations of O (0.95 wt %) and P (2.85 wt %). The enrichment of Fe in the cell wall is likely the result of dissimilatory Fe reduction occurring at the outer membrane by metal-reducing proteins called cytochromes, while the P signal is contributed by typical cellular constituents such as DNA, RNA, and phospholipids (*25*). Therefore, the immediate precipitation of Pb enriched nanoparticles associated with *S. putrefaciens* CN32 at the start of the experiment (Figure 2B) coupled with the presence of Pb in the cell wall and cytoplasm suggests a simultaneous mechanism involving rapid Pb sorption onto the cell wall and intracellular uptake and precipitation (*24, 26, 27*).

While *Shewanella putrefaciens* CN32 has previously demonstrated intracellular precipitation of mixed-valence iron and manganese oxides, this is the first report of intracellular Pb precipitation (*11, 28, 29*). Several bacterial species such as *Citrobacter sp.* and *Staphylococcus aureus* have demonstrated intracellular Pb precipitation (*27, 30, 31*), however, due to the analytical limitations imposed by the small size of the Pb inclusions (<100 nm), detailed analyses of intracellular Pb precipitates are rare. Aside from one reported case of PbS intracellular precipitation by *Klebsiella sp* (*32*), the majority of studies show enrichment of Pb and P within the intracellular granules (*26, 27, 30*) and are identified as either amorphous Pb-polyphosphate (*27*) or crystalline Pb phosphate (*30, 33*).

Polyphosphates (poly P) are linear orthophosphate polymers that serve as energy and phosphorus reservoirs in many microorganisms and are implicated to play a key role in the detoxification of metals such as Cd, Cu, Pb, and U (*34*−*36*). While potassium polyphosphate formation was recently suggested in *Shewanella putrefaciens* CN32, to the best of our knowledge it has not been confirmed microscopically (*11, 37*). In contrast to other studies demonstrating Pb-polyphosphate formation, HR-TEM images of the precipitates in our study reveal a crystalline structure thereby suggesting inorganic lead phosphate formation rather than amorphous polyphosphate formation (Figure 3B and SI Figure S6). Moreover, the relative concentration of P is lower than the amount of Pb thus conflicting with similar analyses of bacterial polyphosphate inclusions where P is high (SI Table

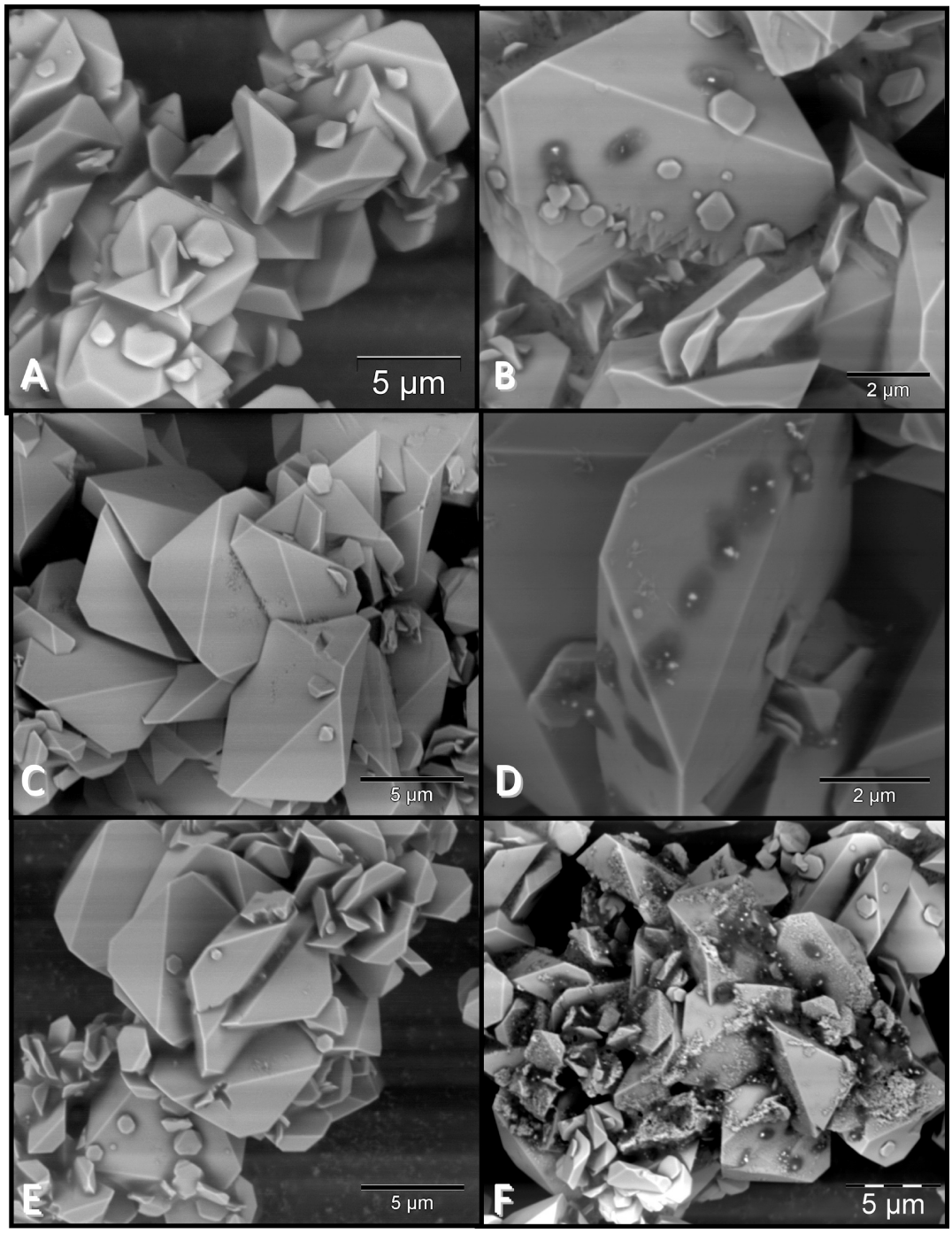

FIGURE 2. BSE-SEM images of control Pb-jarosite (left) and inoculated Pb-jarosite (right) as a function of time; (A) and (B) =0 h, (C) and (D) = 16 h, (E) and (F) = 768 h.

S5) (*38*). Finally, while previous studies illustrate polyphosphate degradation under anaerobic conditions, our study demonstrates intracellular Pb phosphate formation under anaerobic conditions thereby eliminating the possibility for polyphosphate formation in our bacteria (*36*).

A potential explanation for Pb phosphate precipitation by *Shewanella putrefaciens* CN32 may be attributed to heavy metal translocating P_{IB}-type ATPases (COG2217P), a superfamily of enzymes responsible for metal ion efflux and resistance in cells. P_{IB}-type ATPases bind divalent metals such as Pb, Cd, and Zn to the N-terminal amino acid domain of the enzyme and also catalyze ATP hydrolysis. The energy produced during ATP hydrolysis is used to actively transport the metal complex out of the cytoplasm. Contained within the genome of *Shewanella putrefaciens* CN32 is ZntA (Sputcn32_1954), a metal-translocating ATPase, previously shown to expel Pb(II), Cd(II), and Zn(II) from cells of *Escherichia coli*. Also found within the genome of *Shewanella putrefaciens* CN32 is ZntR (Sputcn32_3400), a member of the MerR family of transcriptional regulators (COG0789K) encoded to activate *zntA* expression in the presence of Pb, Cd, and Zn(II) (*39*). Previous results showed that soft metal complexes stimulated the ATPase activity of purified ZntA in the order Pb(II) > Cd(II) ~ Zn(II) ~ Hg(II) thus suggesting that ZntA was a Pb(II)-dependent ATPase evolved specifically to mediate resistance to toxic concentrations of environmental Pb (*39*). It may be expected that in the presence of high Pb concentrations within the cell, ZntR will induce ZntA synthesis and Pb will be transported out of the cell. However, in this study the Pb remained within the cytoplasm which

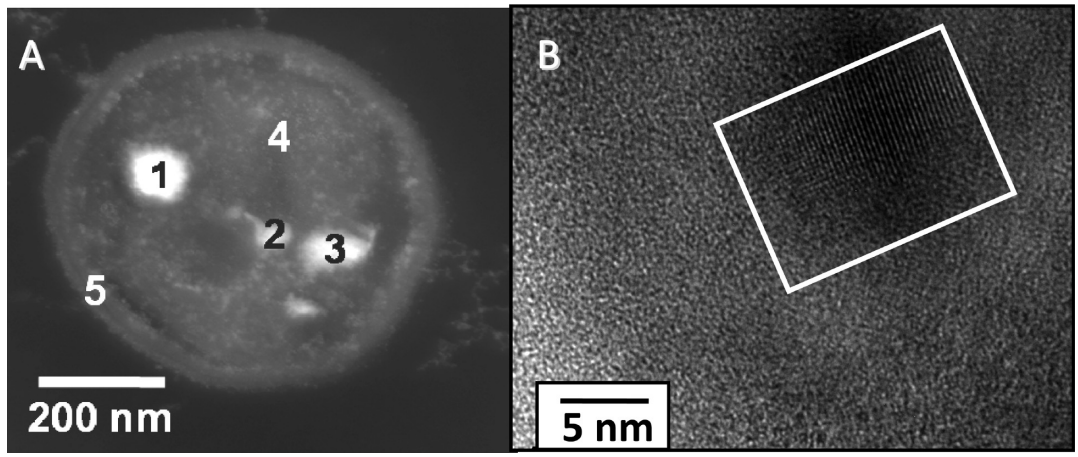

FIGURE 3. (A) TEM images of a cross section of *Shewanella putrefaciens*. Numbers 1−5 denote areas of EDS analysis. (B) HR-TEM image of an electron dense intracellular precipitate. Square denotes area of crystallinity.

is likely due to complexation with the P released from ATP hydrolysis followed by rapid precipitation of a highly insoluble Pb phosphate phase ($K_{sp} = 10^{-54}$) (*40*).

The absence of P in the minimal media may also have played an important role in the intracellular Pb mineralization observed in *S. putrefaciens* CN32. A previous study using *Pseudomonas fluorescens* examined Pb accumulation under P limited and rich conditions and demonstrated intracellular Pb accumulation in P limited media and extracellular Pb accumulation in P rich media (*41*). Due to the insolubility of Pb phosphate and the potential for P surface complexation onto the Pb-jarosite, P was not added to the minimal media. However, it may be possible that due to the reduced ATP production as a result of Pb toxicity and P starvation, the energy released during ATP hydrolysis may have been insufficient to expel the Pb out of the cytoplasm. P is of particular interest because it is often limiting to microbial growth in natural aqueous environments. However, due to the absence of reaction vessels containing P, the interplay between cellular P nutrition, Fe reduction and Pb detoxification by *S. putrefaciens* CN32 remains to be delineated.

Interestingly, the anaerobic dissolution of silver-jarosite by the same stock culture of *S. putrefaciens* CN32, demonstrated a different mechanism for silver detoxification (*10*). During Ag-jarosite dissolution, reduced Ag nanoparticles precipitated along the inner plasma membrane of the cell rather than inside the cytoplasm as was illustrated in this study. A potential explanation for this difference may be in the genome as the *Shewanella putrefaciens* CN32 genome also encodes for a putative silver efflux pump (Sputcn32_0149), a member of the CzcA family of heavy metal efflux proteins. Gene expression was not measured in this study, therefore the role of P-type ATPase expression or other metal efflux pumps responsible for Pb and Ag detoxification by *Shewanella putrefaciens* CN32 remains to be elucidated.

The results of this study demonstrate enhanced dissolution of Pb-jarosite by *S. putrefaciens* CN32 through dissimilatory Fe reduction under anaerobic circumneutral conditions. The dissolution of the control and inoculated Pb-jarosite samples both showed aqueous Pb release followed by immobilization either onto the secondary precipitate or within the bacteria. This study demonstrates the first case of intracellular precipitation of an enriched Pb and P mineral phase by *Shewanella putrefaciens* CN 32. Intracellular Pb-polyphosphate formation was recently observed for the first time in nature in unidentifiable bacteria collected from a vineyard and forest site in France (*27*). Therefore, this newly reported Pb biomineralization pathway in *S. putrefaciens* CN32 may represent a significant sink for Pb in the environment and should be considered when evaluating future remediation options in Pb contaminated sites. In the absence of samples supplemented with P, the effect of P limitation on the uptake and intracellular accumulation of Pb remains to be delineated and should be the focus of future research. Lastly, while *S. putrefaciens* CN32 is a well-characterized and commonly used bacteria to model dissimilatory Fe reduction, future studies should assess the reductive dissolution of Pb-jarosite using other environmentally relevant bacterial strains. It is expected that experiments using a suite of other environmentally relevant bacteria such as *Geobacter sp.* would provide a more comprehensive and accurate assessment of the potential for Pb release from Pb-jarosite into the environment.

Acknowledgments

We gratefully acknowledge the financial support of NSERC (Discovery Grant Nos. 83117 and 860006). We thank Marcia Reid (Health Science Centre) and Carmen Andrei (Brockhouse Institute for Materials Research), at McMaster University for their valuable TEM preparation and analysis assistance. We also thank J.C. Barrette, Sharon Lackie, Siddharth Joshi, Steve Holland, and Lei Zhang at GLIER for analysis assistance.

Supporting Information Available

Additional details including: synthesis of Pb-jarosite, preparation *S. putrefaciens* suspensions; aqueous sampling procedures; SEM and TEM preparation and analysis; cell viability analysis; XRD pattern for Pb-jarosite; SE and BSE-SEM images and EDS analysis of secondary precipitates; Additional TEM and HR-TEM images of cells and cell mineral aggregates, Eh measurements; Cell luminosity data and geochemical modeling parameters/ results. This material is available free of charge via the Internet at http://pubs.acs.org.

Literature Cited

(1) Dutrizac, J. E.; Jambor, J. L. Jarosites and their application in hydrometallurgy. In *Sulfate Minerals—Crystallography, Geochemistry and Environmental Significance*, Reviews in Mineralogy & Geochemistry; Alpers, C N., Jambor, J. L., Nordstrom, D. K., Eds.; Mineralogical Society of America and Geochemical Society: Chantilly, VA, 2000; Vol. 40, pp 405−452.

(2) Hudson-Edwards, K. A.; Schell, C.; Macklin, M. G. Mineralogy and geochemistry of alluvium contaminated by metal mining in the Rio Tinto area, southwest Spain. *Appl. Geochem.* **1999**, *14* (8), 1015–1030.

(3) Chapman, B. M.; Jones, D. R.; Jung, R. F. Processes controlling metal-ion attenuation in acid-mine drainage streams. *Geochim. Cosmochim. Acta* **1983**, *47* (11), 1957–1973.

(4) Hochella, M. F.; Moore, J. N.; Golla, U.; Putnis, A. A TEM study of samples from acid mine drainage systems: Metal-mineral association with implications for transport. *Geochim. Cosmochim. Acta* **1999**, *63* (19−20), 3395–3406.
(5) Smith, A. M. L.; Dubbin, W. E.; Wright, K.; Hudson-Edwards, K. A. Dissolution of lead- and lead-arsenic-jarosites at pH 2 and 8 and 20 degrees C: Insights from batch experiments. *Chem. Geol.* **2006**, *229* (4), 344–361.
(6) Jambor, J. L. Nomenclature of the alunite supergroup. *Can. Mineral.* **1999**, *37*, 1323–1341.
(7) Welch, S. A.; Christy, A. G.; Kirste, D.; BeaviS, S. G.; Beavis, F. Jarosite dissolution I—Trace cation flux in acid sulfate soils. *Chem. Geol.* **2007**, *245* (3−4), 183–197.
(8) Smith, A. M. L.; Hudson-Edwards, K. A.; Dubbin, W. E.; Wright, K. Dissolution of jarosite [KFe3(SO4)(2)(OH)(6)] at pH 2 and 8: Insights from batch experiments and computational modelling. *Geochim. Cosmochim. Acta* **2006**, *70* (3), 608–621.
(9) Bridge, T. A. M.; Johnson, D. B. Reductive dissolution of ferric iron minerals by Acidiphilium SJH. *Geomicrobiol. J.* **2000**, *17* (3), 193–206.
(10) Weisener, C. G.; Babechuk, M. G.; Fryer, B. J.; Maunder, C. Microbial dissolution of silver jarosite: Examining its trace metal behaviour in reduced environments. *Geomicrobiol. J.* **2008**, *25* (7−8), 415–424.
(11) Glasauer, S.; Langley, S.; Boyanov, A.; Lai, B.; Kemner, K.; Beveridge, T. J. Mixed-valence cytoplasmic iron granules are linked to anaerobic respiration. *Appl. Environ. Microbiol.* **2007**, *73* (3), 993–996.
(12) Roden, E. E. Fe(III) oxide reactivity toward biological versus chemical reduction. *Environ. Sci. Technol.* **2003**, *37* (7), 1319–1324.
(13) Fredrickson, J. K.; Zachara, J. M.; Kennedy, D. W.; Dong, H. L.; Onstott, T. C.; Hinman, N. W.; Li, S. M. Biogenic iron mineralization accompanying the dissimilatory reduction of hydrous ferric oxide by a groundwater bacterium. *Geochim. Cosmochim. Acta* **1998**, *62* (19−20), 3239–3257.
(14) Dutrizac, J. E. The Precipitation of lead jarosite from chloride media. *Hydrometallurgy* **1991**, *26* (3), 327–346.
(15) Dutrizac, J. E. The behaviour of the rare earths during the precipitation of sodium, potassium and lead jarosites. *Hydrometallurgy* **2004**, *73* (1−2), 11–30.
(16) Viollier, E.; Inglett, P. W.; Hunter, K.; Roychoudhury, A. N.; Van Cappellen, P. The ferrozine method revisited: Fe(II)/Fe(III) determination in natural waters. *Appl. Geochem.* **2000**, *15* (6), 785–790.
(17) Stookey, L. L. Ferrozine - a new spectrophotometric reagent for iron. *Anal. Chem.* **1970**, *42* (7), 779–&.
(18) Ford, R. G.; Bertsch, P. M.; Farley, K. J. Changes in transition and heavy metal partitioning during hydrous iron oxide aging. *Environ. Sci. Technol.* **1997**, *31* (7), 2028–2033.
(19) O'Loughlin, E. J.; Larese-Casanova, P.; Scherer, M.; Cook, R. Green rust formation from the bioreduction of gamma-FeOOH (lepidocrocite): Comparison of several Shewanella species. *Geomicrobiol. J.* **2007**, *24* (3−4), 211–230.
(20) Glasauer, S.; Weidler, P. G.; Langley, S.; Beveridge, T. J. Controls on Fe reduction and mineral formation by a subsurface bacterium. *Geochim. Cosmochim. Acta* **2003**, *67* (7), 1277–1288.
(21) Sturm, A.; Crowe, S. A.; Fowle, D. A. Trace lead impacts biomineralization pathways during bacterial iron reduction. *Chem. Geol.* **2008**, *249* (3−4), 282–293.
(22) Jones, E. J. P.; Nadeau, T. L.; Voytek, M. A.; Landa, E. R. Role of microbial iron reduction in the dissolution of iron hydroxysulfate minerals. *J. Geophys. Res., [Biogeosci.]* **2006**, *111* (G1), xxxx.
(23) Fein, J. B.; Daughney, C. J.; Yee, N.; Davis, T. A. A chemical equilibrium model for metal adsorption onto bacterial surfaces. *Geochim. Cosmochim. Acta* **1997**, *61* (16), 3319–3328.
(24) Templeton, A. S.; Trainor, T. P.; Spormann, A. M.; Newville, M.; Sutton, S. R.; Dohnalkova, A.; Gorby, Y.; Brown, G. E. Sorption versus biomineralization of Pb(II) within *Burkholderia cepacia* biofilms. *Environ. Sci. Technol.* **2003**, *37* (2), 300–307.
(25) Fredrickson, J. K.; Romine, M. F.; Beliaev, A. S.; Auchtung, J. M.; Driscoll, M. E.; Gardner, T. S.; Nealson, K. H.; Osterman, A. L.; Pinchuk, G.; Reed, J. L.; Rodionov, D. A.; Rodrigues, J. L. M.; Saffarini, D. A.; Serres, M. H.; Spormann, A. M.; Zhulin, I. B.; Tiedje, J. M. Towards environmental systems biology of Shewanella. *Nat. Rev. Microbiol.* **2008**, *6* (8), 592–603.
(26) Levinson, H. S.; Mahler, I.; Blackwelder, P.; Hood, T. Lead resistance and sensitivity in Staphylococcus aureus. *FEMS Microbiol. Lett.* **1996**, *145* (3), 421–425.
(27) Perdrial, N.; Liewig, N.; Delphin, J. E.; Elsass, F. TEM evidence for intracellular accumulation of lead by bacteria in subsurface environments. *Chem. Geol.* **2008**, *253* (3−4), 196–204.
(28) Glasauer, S.; Langley, S.; Beveridge, T. J. Intracellular iron minerals in a dissimilatory iron-reducing bacterium. *Science.* **2002**, *295* (5552), 117–119.
(29) Glasauer, S.; Langley, S.; Beveridge, T. J. Intracellular manganese granules formed by a subsurface bacterium. *Environ. Microbiol.* **2004**, *6* (10), 1042–1048.
(30) Aickin, R. M.; Dean, A. C. R.; Cheetham, A. K.; Skarnulis, A. J. Electron-Microscope Studies on the Uptake of Lead by a Citrobacter Species. *Microbios Lett.* **1978**, *9* (33), 7–15.
(31) Tornabene, T. G.; Edwards, H. W. Microbial uptake of lead. *Science* **1972**, *176* (4041), 1334–&.
(32) Aiking, H.; Govers, H.; Vantriet, J. Detoxification of mercury, cadmium, and lead in *Klebsiella aerogenes* Nctc-418 growing in continuous culture. *Appl. Environ. Microbiol.* **1985**, *50* (5), 1262–1267.
(33) Mire, C. E.; Tourjee, J. A.; O'Brien, W. F.; Ramanujachary, K. V.; Hecht, G. B. Lead precipitation by *Vibrio harveyi*: Evidence for novel quorum-sensing interactions. *Appl. Environ. Microbiol.* **2004**, *70* (2), 855–864.
(34) Omelon, S. J.; Grynpas, M. D. Relationships between polyphosphate chemistry, biochemistry, and apatite biomineralization. *Chem. Rev.* **2008**, *108* (11), 4694–4715.
(35) Suzuki, Y.; Banfield, J. F. Resistance to, and accumulation of, uranium by bacteria from a uranium-contaminated site. *Geomicrobiol. J.* **2004**, *21* (2), 113–121.
(36) Vanveen, H. W.; Abee, T.; Kortstee, G. J. J.; Konings, W. N.; Zehnder, A. J. B. Substrate-specificity of the 2 phosphate-transport systems of acinetobacter-johnsonii-210a in relation to phosphate speciation in its aquatic environment. *J. Biol. Chem.* **1994**, *269* (23), 16212–16216.
(37) Krause, B.; Beveridge, T. J.; Remsen, C. C.; Nealson, K. H. Structure and properties of novel inclusions in Shewanella putrefaciens. *FEMS Microbiol. Lett.* **1996**, *139* (1), 63–69.
(38) Webster, J. A.; Fay, D. D.; Costa, J. L.; Jones, P. M.; Hugh, R. Elemental composition of bacterial metachromatic inclusions determined by electron-microprobe X-ray-analysis. *J. Bacteriol.* **1984**, *158* (2), 441–446.
(39) Sharma, R.; Rensing, C.; Rosen, B. P.; Mitra, B. The ATP hydrolytic activity of purified ZntA, a Pb(II)/Cd(II)/Zn(II)-translocating ATPase from *Escherichia coli*. *J. Biol. Chem.* **2000**, *275* (6), 3873–3878.
(40) Nies, D. H. Microbial heavy-metal resistance. *Appl. Microbiol. Biotechnol.* **1999**, *51* (6), 730–750.
(41) Al-Aoukaty, A.; Appanna, V. D.; Huang, J. Exocellular and intracellular accumulation of lead in *Pseudomonas-fluorescens* Atcc-13525 is mediated by the phosphate content of the growth-medium. *FEMS Microbiol. Lett.* **1991**, *83* (3), 283–290.

ES901629C